Transient State Measurements on Proteins by Time-Resolved Crystallography

Tek Narsingh Malla, Marius Schmidt

University of Wisconsin-Milwaukee, Physics Department, Milwaukee, USA

Abstract

After decades of diligent development at synchrotron light sources, the field of time-resolved crystallography (TRX) is elevating to new heights. Driven by the appearance of X-ray free electron lasers and supported by serial crystallography, a large number of biological systems can now be investigated with TRX. This short review cannot comprehensively cover all of them, but it will shine light on, and provide a connection between, some of the recent and past results.

Short Title: Advances in Time-Resolved Crystallography

Highlights:

X-ray Free Electron Lasers promote femtosecond time-resolution

Transitions through conical intersections can be visualized with single femtosecond precision

The mechanics of chloride-pumping is revealed in a chloride ion pumping rhodopsin

The complete Z to E isomerization in a biliprotein has been revealed by time-resolved crystallography

The structures of transient states can be directly determined from enzyme catalyzed reactions by diffusion of substrate into microcrystals.

Keywords:

Time resolved (serial femtosecond) crystallography, photoactive yellow protein, chloride and sodium ion pumping rhodopsins, bacteriophytochromes, mix-and-inject serial crystallography

Intermediate States

Life is made possible by chemical reactions that are promoted by biological macromolecules. Many proteins possess catalytic (or enzymatic) activity necessary to perform the functions of life. Chemical reactions advance from fundamental, ultrashort events through reaction intermediates (RI) to the formation of a product on longer time scales. A RI results from a significant minimum in the energy landscape (EL) (Fig. 1 b) of a biological macromolecule, and its lifetime should be much longer than a molecular vibration[1]. Although casually used, the lifetime of an intermediate is a misnomer. An intermediate state is visited or occupied by an ensemble of reacting molecules. Accordingly, in this context, the lifetime is equivalent to the characteristic time an intermediate state is occupied. The timescale of a molecular vibration in proteins spans from tens of femtoseconds (tens of terahertz, THZ) for very localized vibrations to picoseconds for long range, global fluctuations with energies smaller than 4 meV (< 1 THz)[2,3]. Given the above definition, it is hard to envision a protein RI that is populated on a time scale much faster than a few ps, unless very localized dynamics is considered. The EL of a biomolecule is complex[4,5]. Relaxations between RIs might be non-exponential[4,6-8]. A large number of shallow energy minima along the reaction pathway may exist that are not visited long enough by reacting molecules that measurable occupancy can accumulate. This can make observations of protein RIs difficult. However, if the EL is sufficiently simple[9] (Fig. 1 b), a substantial fraction of reacting molecules can accumulate in distinct RIs. The dynamics of the molecular ensemble can then be characterized (Fig. 1 a, c, d) by using transient state (TS) measurements [10], results of which are interpreted by chemical kinetics [11]. On ultrafast time scales different approaches are required (see e.g. below for the photoactive yellow protein), since not enough time is available to the molecular ensemble to kinetically de-phase. Usually, multiple RIs are occupied simultaneously at most time-points of the TS measurements. These mixtures need to be separated to determine the physical properties (spectra, structures) of pure, admixture free intermediate states. The time information inherent in time-resolved data can be exploited computationally to achieve this separation [12-16].

Time-Resolved Crystallography at Synchrotron and XFELs

Reactions in biomolecules can be followed with near atomic resolution by TRX[17]. Initially, the 100 ps X-ray pulses at synchrotron light sources were limiting the time-resolution[18-22]. Free

Electron Laser X-ray sources (XFELs)[23] greatly extended this limit to the femtosecond (fs) regime[24-26]. Armed with this toolbox, biological reactions can now be investigated in hitherto unimaginable detail. For a TRX experiment, a reaction must be initiated (triggered) in the crystalline ensemble by a short perturbation which is typically a light pulse, but this can also be achieved by other means such as an increase in temperature[27], by diffusion of substrate [28], or even an electric field pulse[29]. The progress of the reaction is probed by X-ray pulses through a succession of time delays Δt after initiation. With the development of serial crystallography at XFELs[30-32] and its application at synchrotron sources[33-35] TRX gained unprecedented popularity since very challenging problems could finally be solved[36]. Here, a representative assortment of these experiments is reviewed.

Trans to Cis isomerizations

Photoactive Yellow Protein. The function of the photoactive yellow protein (PYP) naturally depends on light. Conformational changes triggered by the absorption of blue light ($\lambda \sim 450$ nm) are believed to be responsible for a behavioral change of the bacteria[37]. Light illumination results in the *trans* to *cis* isomerization of the central *para*-coumaric acid (pCA) chromophore that rotates about the C_2=C_3 ($\Delta_{2,3}$) double bond (Fig. 2 a). Isomerization reactions are very important in chemistry[38] and fundamental to the living world[39]. The isomerization triggers a photocycle (Fig. 1 a). Several RIs (Fig. 1 a)[14,21,22,40] with increasing lifetimes have been identified and characterized by TRX. A giant leap forward was the application of time-resolved serial femtosecond crystallography (TR-SFX)[24] at the Linac Coherent Light Source (LCLS). There, the *trans* to *cis* isomerization of the pCA has been observed in PYP with a time-resolution of about 100 fs[26]. The fs time-range was covered by about 320,000 indexed diffraction pattens. By sorting intensities originating from similar pump-probe delays into time-bins, complete crystallographic datasets that covered the fs time range were obtained[26]. From these datasets difference electron density maps were calculated which characterized the isomerization directly by shifting electron density clouds, and ultimately structures that relax on the fs time-scale. Relaxations are driven by electronic interactions on both the excited state potential energy surface (ES-PES) and the ground state (GS)-PES of the pCA. The *trans* to *cis* isomerization occurs at around 600 fs after photo-initiation (Fig. 2 b), when exited state wave-packets transition through a conical intersection (CI) to the electronic ground state[26]. Recently, the

transition through the CI in PYP has been re-examined by applying a manifold-based machine learning (ML) algorithm[41] to the raw, highly partial, fs time-dependent intensities collected earlier[26,41]. The algorithm greatly enhanced the precision with which the data can be analyzed to a few fs[41]. This way, one can show that the molecular ensemble crosses the CI at 615 fs. The application of the ML algorithm yields four significant spatial modes (reaction coordinates) and corresponding temporal modes that are required to explain the transition. Although these modes were not assigned structurally, one can surmise that two of them are likely associated with the bending of the chromophore along its axis, and the rotation about the $\Delta_{2,3}$ double bond, respectively, as noted earlier[26]. However, from individual modes difference electron density maps can be calculated and combined to movies with few-fs frame rate which give an impression how the pCA structure changes when crossing the CI. Trajectories through the CI were further explored by a quantum mechanical (QM) calculation whose parameters could be tied directly to the experiment by fitting the result of the QM calculation to the significant modes provided by the ML algorithm[41]. This then results in a fs movie that pictures the wavepacket dynamics from the ES-PES to the GS-PES through the CI. After the CI (around 800 fs) the pCA is observed in a twisted *cis* configuration that relaxes further on the GS-PES. At about 3 ps, a first photocycle intermediate can be identified with the pCA very close to the *cis*-configuration. (Fig. 2 c). Its structure is already similar to the early intermediate I_T (Fig. 1 a) observed by synchrotron Laue experiments at around 100 ps [21,22,42].

Bacteriorhodopsin. Bacteriorhodopsin (BR) is a model system for light driven reactions. The reaction is caused by the *trans* to *cis* isomerization of its retinal chromophore[43]. The retinal is bound to a lysine forming a Schiff base (Fig. 2 d). BR displaces protons from the inside, across the cell membrane to the outside of bacteria. The resulting proton gradient is used to fuel the bacteria's life-functions. Although extensively investigated, TRX structures were elusive until XFELs became available. BR microcrystals are exquisitely well suited for TR-SFX. Small crystals allow uniform penetration by laser light[24,26,44] that maximizes reaction initiation and population transfer. This made it possible to characterize the fundamental $\Delta_{13,14}$ *trans* to *cis* isomerization of the retinal[45,46]. The combination of TR-SFX at slower time-scales[47] and time-resolved synchrotron serial crystallography (TR-SSX)[48] was employed to structurally characterize RIs during the complete BR photocycle. Furthermore, reactions in cation (Na^+) and anion (Cl^-) pumping rhodopsins (Fig. 1 d) were investigated[49,50]. The advantage is that

electron densities of the ions (Na^+: 10 e^-, Cl^-: 18 e^-) can be identified whereas the H^+ in BR remains invisible to X-rays. The Cl^- (but not the Na^+) initially interacts with the positively charged Schiff-base (Fig. 2 e). During isomerization the Schiff-base releases the Cl^- that is then free to move to the other side of the membrane[50]. Since Na^+ is not bound to the Schiff base in the Na^+ pump, its locations are difficult to identify, but they have been inferred with the help of site specific mutations and computational approaches[49]. Subsequent conformational changes of the respective rhodopsins assist in transferring the pumped ions across the membrane[49,50].

Phytochromes. Photochromes are red light receptors found in plant, bacteria and fungi[51]. Although phytochromes are structurally diverse, most of them harbor a photosensory core module (PCM, about 75 kDa) that reacts with light and transfers the signal to an effector domain with enzymatic activity. In bacteriophytochromes (BphP) the light is absorbed by a covalently bound biliverdin (BV), an open chain tetrapyrrole located in the PCM (Fig. 3 b). A typical phytochrome rests in a red-light absorbing state called Pr. Upon illumination with red light, the BV D-ring isomerizes about the $\Delta_{15,16}$ double bond (Fig. 3 b) from a *cis* configuration (*Z* for 'zusammen, together') to a *trans* configuration (*E* for 'entgegen, distant'). The *Z* to *E* isomerization drives one half of a photocycle with several intermediates (Fig. 1 c) that ends in a stable conformation called P_{fr} that absorbs in the far-red. Illumination with far-red light causes the D-ring to flip back to the *Z* form, after which the phytochrome relaxes towards P_r (Fig. 1 c). The isomerization is sensed by an enzymatic domain covalently attached to the PCM whose activity is light controlled this way. Full length BphP crystals are difficult to obtain. Therefore, truncated constructs that consists of the PCM or the even smaller chromophore binding domain (CBD) are crystallized. Microcrystals of the *Deinococcus radiodurans* DrBphP CBD[52] and those of the *Stigmatella aurantica* SaBphP2 PCM[53,54] diffract exquisitely well at XFELs with resolutions at or better than 2 Å[52,53,55] which makes them well suited for TR-SFX experiments. Rotations of BV ring-D were first identified by TR-SFX experiments at the Japanese XFEL Spring-8 Ångstrom Compact X-ray Laser (SACLA) on the smaller CBD fragment[56]. The CBD is only transiently photoreactive as it quickly (< 1 ns) relaxes back to the dark state. Surprisingly, the so-called pyrrole water (see Fig. 3 c for its location) is photo-ejected within 1 ps. The BV D-ring rotates about 50° in a counterclockwise direction. At the same time the chromophore's hydrogen bonds to the surrounding protein matrix are disrupted. As a result, already at 1 ps substantial difference electron density is observed up to 15 Å from the pyrrole

water [56]. The larger SaBphP2 PCM is weakly photostable and crystals diffracts to record high resolution[53]. With nanosecond TR-SFX, performed also at SACLA, RI structures at 5 ns (Fig. 3 a) and 33 ms were obtained[54]. Similar to the DrBphP CBD, the pyrrole water is photo-ejected (Fig. 3 c). But in contrast to the CBD, ring D rotates clockwise by 180^{o} (Fig. 3 c) in the PCM thereby completing the *Z* to *E* isomerization. The PHY domain that is present in the PCM but not in the CBD is in direct contact with the chromophore via an extension called the sensory tongue (Fig. 3 a). This may be the cause for the differences in the structural responses between both constructs. At 5 ns the chromophore adopts a twisted configuration and is displaced by several Å. This results in structural changes that distribute across the protein into the PHY domain (Fig. 3 a). Large scale structural changes of the PHY domains which were observed in other, static structures[57], are not observed even at a 33 ms pump-probe delay. It is not clear whether this is a consequence of crystal lattice contacts, or whether the structure continues to evolve beyond 33 ms. Further experiments at longer time delays are required.

Enzymology with the Mix-and-Inject Technique

TRX experiments on enzymes are rare with exceptions[58,59] in particular when an inactive, caged substrate is available that can be activated by a laser pulse[60-62]. A more general method to trigger reactions in enzymes is diffusion which only requires mixing of crystals with substrate[28,63,64]. This idea was initially pursued by researchers using crystals with edge lengths of hundreds of μm[65]. Diffusion times were much longer than the turnover rate of even relatively slow enzymes[66]. This changed substantially when XFELs became available. High resolution diffraction patterns can be collected from micron and sub-micron sized crystals[67]. The crystals are thin in all three dimensions which greatly shorten diffusion times[28]. Due to the 'diffraction-before-destruction' principle[68], radiation damage is not critical. Diffusion follows Fick's laws. Solutions exist for several three dimensional shapes[69] with which substrate concentrations in protein crystals can be calculated[28,70]. Substrate binding and the catalytic reaction of the enzyme β-lactamase (BlaC, Fig. 4 a) from *M. tuberculosis* with a cephalosporin antibiotic has been investigated at the LCLS[71] and the European XFEL (EuXFEL)[72] (Fig. 4 d-i). As a result, an apparent diffusion coefficient of the substrate in the crystalline environment, the time and space dependent substrate concentrations as well as their occupancies could be deduced experimentally everywhere in the crystal and at any time (Fig. 4 b, c). After about 30

ms, the formation of the enzyme-substrate complex is complete (Fig. 4 g). About 500 ms later, the so-called acyl-RI is observed[71] (Fig. 4 i) which is critical for antibiotics inactivation. A practical method now exists to observe biologically and biomedically relevant reactions with TRX[70] provided that microcrystals and soluble substrate are available.

XFELs and Synchrotron Light Sources

Mixing experiments were conducted with mix-and-inject serial crystallography at XFELs[71,73-77] and using fixed targets at the synchrotron[78,79]. Since a large number of diffraction patterns is required, it is desirable to identify a method to substantially reduce this number for the swift collection of complete datasets. By increasing the bandwidth of the X-ray radiation, all or a substantial part of the integrated reflection intensity is collected from a still exposure[80]. This reduces the number of diffraction pattern necessary[81,82]. When crystals smaller than about 10 μm are used for mixing experiments, it is important to tightly focus the X-ray beam and to expose longer. This may become possible with new storage ring designs that promise sub-10 μm focal spots[83,84]. The experiment can then be performed with smaller crystals with few μs exposure times. SFX and SSX were compared at the EuXFEL and the synchrotron Petra-III, respectively, with the conclusion that data of comparable quality can be obtained[85]. However, when carbonmonoxy myoglobin, a heme protein, is investigated with SSX[85], difference density features appeared on and near the heme iron which is indicative of a change of the oxidation state of the metal. Further experiments are necessary to home-in on this effect. Crystallography will transition (has already moved) from the determination of static structures to the collection of time series with closely spaced time delays that span an entire reaction pathway from fundamental events to the formation of product, from which RIs can be extracted. The next grand challenge is to predict both structure and dynamics from protein sequences[86]. To generate the required data base, it is essential that XFELs and synchrotron light sources are available to a wide community to guarantee access to latest technology and continuing innovation.

Acknowledgement

M.S. is supported by the NSF-STC 'Biology with XFELs (BioXFEL)', award number STC-1231306.

Literature

1. IUPAC: *Compendium of Chemical Terminology, Gold Book*: International Union of Pure and Applied Chemistry; 2014.
2. Achterhold K, Keppler C, Ostermann A, van Burck U, Sturhahn W, Alp EE, Parak FG: **Vibrational dynamics of myoglobin determined by the phonon-assisted Mossbauer effect**. *Physical Review E* 2002, **65**.
3. Niessen KA, Xu MY, George DK, Chen MC, Ferre-D'Amare AR, Snell EH, Cody V, Pace J, Schmidt M, Markelz AG: **Protein and RNA dynamical fingerprinting**. *Nature Communications* 2019, **10**.
4. Austin RH, Beeson KW, Eisenstein L, Frauenfelder H, Gunsalus IC: **Dynamics of ligand binding to myoglobin**. *Biochemistry* 1975, **14**:5355-5373.
5. Wales DJ: *Energy Landscapes, with Applications to Clusters, Biomolecules and Glasses*. Edited by Saykally R, Zewail A, King D. Cambridge: Cambridge University Press; 2003.
6. Bourgeois D, Vallone B, Schotte F, Arcovito A, Miele AE, Sciara G, Wulff M, Anfinrud P, Brunori M: **Complex landscape of protein structural dynamics unveiled by nanosecond Laue crystallography**. *Proc Natl Acad Sci U S A* 2003, **100**:8704-8709.
7. Aranda R, Levin EJ, Schotte F, Anfinrud PA, Phillips GN: **Time-dependent atomic coordinates for the dissociation of carbon monoxide from myoglobin**. *Acta Crystallographica Section D-Structural Biology* 2006, **62**:776-783.
8. Bourgeois D, Vallone B, Arcovito A, Sciara G, Schotte F, Anfinrud PA, Brunori M: **Extended subnanosecond structural dynamics of myoglobin revealed by Laue crystallography**. *Proc Natl Acad Sci U S A* 2006, **103**:4924-4929.
9. Moffat K: **Time-resolved biochemical crystallography: A mechanistic perspective**. *Chem Rev* 2001, **101**:1569-1581.
10. Cornish-Bowden A: *Fundamentals of Enzyme Kinetics* edn 4 edition: Wiley-VCH; 2012.
11. Steinfeld JI, Francisco JS, Hase WL: *Chemical Kinetics and Dynamics* edn 2 edition: Prentience Hall; 1985.
12. Henry ER, Hofrichter J: **Singular Value Decomposition - Application to Analysis of Experimental-Data**. *Methods in Enzymology* 1992, **210**:129-192.
13. Schmidt M, Rajagopal S, Ren Z, Moffat K: **Application of singular value decomposition to the analysis of time-resolved macromolecular X-ray data**. *Biophys J* 2003, **84**:2112-2129.
14. Ihee H, Rajagopal S, Srajer V, Pahl R, Anderson S, Schmidt M, Schotte F, Anfinrud PA, Wulff M, Moffat K: **Visualizing reaction pathways in photoactive yellow protein from nanoseconds to seconds**. *Proc Natl Acad Sci U S A* 2005, **102**:7145-7150.
15. Schmidt M: *Structure based enzyme kinetics by time-resolved X-ray crystallography, in: ultrashort laser pulses in medicine and biology*. Edited by Zinth W, Braun M, Gilch P. Germany: Berlin ; New York : Springer, c2008; 2008.
16. Schmidt M, Srajer V, Henning R, Ihee H, Purwar N, Tenboer J, Tripathi S: **Protein energy landscapes determined by five-dimensional crystallography**. *Acta Crystallogr D Biol Crystallogr* 2013, **69**:2534-2542.
17. Moffat K: **Time-resolved macromolecular crystallography**. *Annu Rev Biophys Biophys Chem* 1989, **18**:309-332.
18. Srajer V, Teng TY, Ursby T, Pradervand C, Ren Z, Adachi S, Schildkamp W, Bourgeois D, Wulff M, Moffat K: **Photolysis of the carbon monoxide complex of myoglobin: Nanosecond time-resolved crystallography**. *Science* 1996, **274**:1726-1729.
19. Perman B, Srajer V, Ren Z, Teng TY, Pradervand C, Ursby T, Bourgeois D, Schotte F, Wulff M, Kort R, et al.: **Energy transduction on the nanosecond time scale: Early structural events in a xanthopsin photocycle**. *Science* 1998, **279**:1946-1950.

20. Schotte F, Lim M, Jackson TA, Smirnov AV, Soman J, Olson JS, Phillips GN, Jr., Wulff M, Anfinrud PA: **Watching a protein as it functions with 150-ps time-resolved x-ray crystallography**. *Science* 2003, **300**:1944-1947.
21. Schotte F, Cho HS, Kaila VR, Kamikubo H, Dashdorj N, Henry ER, Graber TJ, Henning R, Wulff M, Hummer G, et al.: **Watching a signaling protein function in real time via 100-ps time-resolved Laue crystallography**. *Proc Natl Acad Sci U S A* 2012, **109**:19256-19261.
22. Jung YO, Lee JH, Kim J, Schmidt M, Moffat K, Srajer V, Ihee H: **Volume-conserving trans-cis isomerization pathways in photoactive yellow protein visualized by picosecond X-ray crystallography**. *Nat Chem* 2013, **5**:212-220.
23. Pellegrini C: **The development of XFELs**. *Nature Reviews Physics* 2020, **2**:330-331.
24. Tenboer J, Basu S, Zatsepin N, Pande K, Milathianaki D, Frank M, Hunter M, Boutet S, Williams GJ, Koglin JE, et al.: **Time-resolved serial crystallography captures high-resolution intermediates of photoactive yellow protein**. *Science* 2014, **346**:1242-1246.
25. Barends TR, Foucar L, Ardevol A, Nass K, Aquila A, Botha S, Doak RB, Falahati K, Hartmann E, Hilpert M, et al.: **Direct observation of ultrafast collective motions in CO myoglobin upon ligand dissociation**. *Science* 2015, 10.1126/science.aac5492.
26. Pande K, Hutchison CDM, Groenhof G, Aquila A, Robinson JS, Tenboer J, Basu S, Boutet S, Deponte D, Liang M, et al.: **Femtosecond Structural Dynamics Drives the Trans/Cis Isomerization in Photoactive Yellow Protein**. *Science* 2016, **352**:725-729.
27. Thompson MC, Barad BA, Wolff AM, Sun Cho H, Schotte F, Schwarz DMC, Anfinrud P, Fraser JS: **Temperature-jump solution X-ray scattering reveals distinct motions in a dynamic enzyme**. *Nat Chem* 2019, **11**:1058-1066.
28. Schmidt M: **Mix and Inject, Reaction Initiation by Diffusion for Time-Resolved Macromolecular Crystallography**. *Advances on Condensed Matter Physics* 2013:1-10.
29. Hekstra DR, White KI, Socolich MA, Henning RW, Srajer V, Ranganathan R: **Electric-field-stimulated protein mechanics**. *Nature* 2016, **540**:400-405.
30. Chapman HN, Fromme P, Barty A, White TA, Kirian RA, Aquila A, Hunter MS, Schulz J, DePonte DP, Weierstall U, et al.: **Femtosecond X-ray protein nanocrystallography**. *Nature* 2011, **470**:73-77.
31. Boutet S, Lomb L, Williams GJ, Barends TR, Aquila A, Doak RB, Weierstall U, DePonte DP, Steinbrener J, Shoeman RL, et al.: **High-resolution protein structure determination by serial femtosecond crystallography**. *Science* 2012, **337**:362-364.
32. Orville AM: **Recent results in time resolved serial femtosecond crystallography at XFELs**. *Curr Opin Struct Biol* 2020, **65**:193-208.
33. Stellato F, Oberthuer D, Mengning L, Bean R, Gati C, Yefanov O, Barty A, Burkhardt K, P. F, Galli L, et al.: **Room-temperature macromolecular serial crystallography using synchrotron radiation**. *IUCrJ* 2014, **1**:204-212.
34. Martin-Garcia JM: **Protein Dynamics and Time Resolved Protein Crystallography at Synchrotron Radiation Sources: Past, Present and Future** *crystals* 2021, **11**.
35. Pearson AR, Mehrabi P: **Serial synchrotron crystallography for time-resolved structural biology**. *Curr Opin Struct Biol* 2020, **65**:168-174.
36. Branden G, Neutze R: **Advances and challenges in time-resolved macromolecular crystallography**. *Science* 2021, **373**.
37. Sprenger WW, Hoff WD, Armitage JP, Hellingwerf KJ: **The Eubacterium Ectothiorhodospira-Halophila Is Negatively Phototactic, with a Wavelength Dependence That Fits the Absorption-Spectrum of the Photoactive Yellow Protein**. *Journal of Bacteriology* 1993, **175**:3096-3104.
38. Dugave C, Demange L: **Cis-trans isomerization of organic molecules and biomolecules: Implications and applications**. *Chemical Reviews* 2003, **103**:2475-2532.
39. Dugave C: *cis-trans Isomerization in Biochemistry*: Wiley-VCH; 2006.

40. Schmidt M, Pahl R, Srajer V, Anderson S, Ren Z, Ihee H, Rajagopal S, Moffat K: **Protein kinetics: structures of intermediates and reaction mechanism from time-resolved x-ray data**. *Proc Natl Acad Sci U S A* 2004, **101**:4799-4804.
41. Hosseinizadeh A, Breckwoldt N, Fung R, Sepehr R, Schmidt M, Schwander P, Santra R, Ourmzad A: **Single-femtosecond atomic-resolution observation of a protein traversing a conical intersection**. *Nature* 2021, doi.org/10.1101/2020.11.13.382218.
42. Pandey S, Bean R, Sato T, Poudyal I, Bielecki J, Cruz Villarreal J, Yefanov O, Mariani V, White TA, Kupitz C, et al.: **Time-resolved serial femtosecond crystallography at the European XFEL**. *Nat Methods* 2020, **17**:73-78.
43. Wickstrand C, Nogly P, Nango E, Iwata S, Standfuss J, Neutze R: **Bacteriorhodopsin: Structural Insights Revealed Using X-Ray Lasers and Synchrotron Radiation**. *Annu Rev Biochem* 2019, **88**:59-83.
44. Grunbein ML, Stricker M, Nass Kovacs G, Kloos M, Doak RB, Shoeman RL, Reinstein J, Lecler S, Haacke S, Schlichting I: **Illumination guidelines for ultrafast pump-probe experiments by serial femtosecond crystallography**. *Nat Methods* 2020, 10.1038/s41592-020-0847-3.
45. Nogly P, Weinert T, James D, Carbajo S, Ozerov D, Furrer A, Gashi D, Borin V, Skopintsev P, Jaeger K, et al.: **Retinal isomerization in bacteriorhodopsin captured by a femtosecond x-ray laser**. *Science* 2018, **361**:145-+.
46. Kovacs GN, Colletier JP, Grunbein ML, Yang Y, Stensitzki T, Batyuk A, Carbajo S, Doak RB, Ehrenberg D, Foucar L, et al.: **Three-dimensional view of ultrafast dynamics in photoexcited bacteriorhodopsin**. *Nature Communications* 2019, **10**.
47. Nango E, Royant A, Kubo M, Nakane T, Wickstrand C, Kimura T, Tanaka T, Tono K, Song CY, Tanaka R, et al.: **A three-dimensional movie of structural changes in bacteriorhodopsin**. *Science* 2016, **354**:1552-1557.
48. Nogly P, James D, Wang D, White TA, Zatsepin N, Shilova A, Nelson G, Liu H, Johansson L, Heymann M, et al.: **Lipidic cubic phase serial millisecond crystallography using synchrotron radiation**. *IUCrJ* 2015, **2**:168-176.
49. Skopintsev P, Ehrenberg D, Weinert T, James D, Kar RK, Johnson PJM, Ozerov D, Furrer A, Martiel I, Dworkowski F, et al.: **Femtosecond-to-millisecond structural changes in a light-driven sodium pump**. *Nature* 2020, **583**:314-+.
50. Yun JH, Li X, Yue J, Park JH, Jin Z, Li C, Hu H, Shi Y, Pandey S, Carbajo S, et al.: **Early-stage dynamics of chloride ion-pumping rhodopsin revealed by a femtosecond X-ray laser**. *Proc Natl Acad Sci U S A* 2021, **118**.
51. Auldridge ME, Forest KT: **Bacterial phytochromes: More than meets the light**. *Critical Reviews in Biochemistry and Molecular Biology* 2011, **46**:67-88.
52. Edlund P, Takala H, Claesson E, Henry L, Dods R, Lehtivuori H, Panman M, Pande K, White T, Nakane T, et al.: **The room temperature crystal structure of a bacterial phytochrome determined by serial femtosecond crystallography**. *Sci Rep* 2016, **6**:35279.
53. Sanchez JC, Carrillo M, Pandey S, Noda M, Aldama L, Feliz D, Claesson E, Wahlgren WY, Tracy G, Duong P, et al.: **High-resolution crystal structures of amyxobacterial phytochrome at cryo and roomtemperatures**. *Structural Dynamics-Us* 2019, **6**.
54. Carrillo M, Pandey S, Sanchez J, Noda M, Poudyal I, Aldama L, Malla TN, Claesson E, Wahlgren WY, Feliz D, et al.: **High-resolution crystal structures of transient intermediates in the phytochrome photocycle**. *Structure* 2021, 10.1016/j.str.2021.03.004.
55. Woitowich NC, Halavaty AS, Waltz P, Kupitz C, Valera J, Tracy G, Gallagher KD, Claesson E, Nakane T, Pandey S, et al.: **Structural basis for light control of cell development revealed by crystal structures of a myxobacterial phytochrome**. *IUCrJ* 2018, **5**:619-634.
56. Claesson E, Wahlgren WY, Takala H, Pandey S, Castillon L, Kuznetsova V, Henry L, Panman M, Carrillo M, Kubel J, et al.: **The primary structural photoresponse of phytochrome proteins captured by a femtosecond X-ray laser**. *Elife* 2020, **9**.

57. Takala H, Bjorling A, Berntsson O, Lehtivuori H, Niebling S, Hoernke M, Kosheleva I, Henning R, Menzel A, Ihalainen JA, et al.: **Signal amplification and transduction in phytochrome photosensors**. *Nature* 2014, **509**:245-248.
58. Helliwell JR, Nieh YP, Raftery J, Cassetta A, Habash J, Carr PD, Ursby T, Wulff M, Thompson AW, Niemann AC, et al.: **Time-resolved structures of hydroxymethylbilane synthase (Lys59Gln mutant) as it is loaded with substrate in the crystal determined by Laue diffraction**. *Journal of the Chemical Society-Faraday Transactions* 1998, **94**:2615-2622.
59. Sorigue D, Hadjidemetriou K, Blangy S, Gotthard G, Bonvalet A, Coquelle N, Samire P, Aleksandrov A, Antonucci L, Benachir A, et al.: **Mechanism and dynamics of fatty acid photodecarboxylase**. *Science* 2021, **372**.
60. Schlichting I, Almo SC, Rapp G, Wilson K, Petratos K, Lentfer A, Wittinghofer A, Kabsch W, Pai EF, Petsko GA, et al.: **Time-Resolved X-Ray Crystallographic Study of the Conformational Change in Ha-Ras P21 Protein on Gtp Hydrolysis**. *Nature* 1990, **345**:309-315.
61. Stoddard BL, Cohen BE, Brubaker M, Mesecar AD, Koshland DE, Jr.: **Millisecond Laue structures of an enzyme-product complex using photocaged substrate analogs**. *Nat Struct Biol* 1998, **5**:891-897.
62. Mehrabi P, Schulz EC, Dsouza R, Muller-Werkmeister HM, Tellkamp F, Miller RJD, Pai EF: **Time-resolved crystallography reveals allosteric communication aligned with molecular breathing**. *Science* 2019, **365**:1167-1170.
63. Sluyterman LA, de Graaf MJ: **The activity of papain in the crystalline state**. *Biochim Biophys Acta* 1969, **171**:277-287.
64. Wyckoff HW, Doscher M, Tsernoglou D, Inagami T, Johnson LN, Hardman KD, Allewell NM, Kelly DM, Richards FM: **Design of a diffractometer and flow cell system for X-ray analysis of crystalline proteins with applications to the crystal chemistry of ribonuclease-S**. *J Mol Biol* 1967, **27**:563-578.
65. Hajdu J, Acharya KR, Stuart DI, Mclaughlin PJ, Barford D, Oikonomakos NG, Klein H, Johnson LN: **Catalysis in the Crystal - Synchrotron Radiation Studies with Glycogen Phosphorylase-B**. *Embo Journal* 1987, **6**:539-546.
66. Geremia S, Campagnolo M, Demitri N, Johnson LN: **Simulation of diffusion time of small molecules in protein crystals**. *Structure* 2006, **14**:393-400.
67. Oberthuer D, Knoska J, Wiedorn MO, Beyerlein KR, Bushnell DA, Kovaleva EG, Heymann M, Gumprecht L, Kirian RA, Barty A, et al.: **Double-flow focused liquid injector for efficient serial femtosecond crystallography**. *Sci Rep* 2017, **7**:44628.
68. Chapman HN, Caleman C, Timneanu N: **Diffraction before destruction**. *Philosophical Transactions of the Royal Society B-Biological Sciences* 2014, **369**.
69. Carslaw HS, Jaeger JC: *Conduction Heat in Solids* edn 2nd edition. Oxford: Clarendon Press; 1959.
70. Schmidt M: **Reaction Initiation in Enzyme Crystals by Diffusion of Substrate**. *Crystals* 2020, **10**.
71. Olmos JL, Jr., Pandey S, Martin-Garcia JM, Calvey G, Katz A, Knoska J, Kupitz C, Hunter MS, Liang M, Oberthuer D, et al.: **Enzyme intermediates captured "on the fly" by mix-and-inject serial crystallography**. *BMC Biol* 2018, **16**:59.
72. Pandey S, Calvey G, Katz AM, Malla TN, Koua FHM, Martin-Garcia JM, Poudyal I, Yang JH, Vakili M, Yefanov O, et al.: **Observation of substrate diffusion and ligand binding in enzyme crystals using high-repetition-rate mix-and-inject serial crystallography**. *IUCrJ* 2021, **8**:878-895.
73. Stagno JR, Liu Y, Bhandari YR, Conrad CE, Panja S, Swain M, Fan L, Nelson G, Li C, Wendel DR, et al.: **Structures of riboswitch RNA reaction states by mix-and-inject XFEL serial crystallography**. *Nature* 2017, **541**:242-246.
74. Kupitz C, Olmos JL, Jr., Holl M, Tremblay L, Pande K, Pandey S, Oberthur D, Hunter M, Liang M, Aquila A, et al.: **Structural enzymology using X-ray free electron lasers**. *Struct Dyn* 2017, **4**:044003.

75. Dasgupta M, Budday D, de Oliveira SHP, Madzelan P, Marchany-Rivera D, Seravalli J, Hayes B, Sierra RG, Boutet S, Hunter MS, et al.: **Mix-and-inject XFEL crystallography reveals gated conformational dynamics during enzyme catalysis**. *Proc Natl Acad Sci U S A* 2019, 10.1073/pnas.1901864116.
76. Ramakrishnan S, Stagno JR, Conrad CE, Ding J, Yu P, Bhandari YR, Lee YT, Pauly G, Yefanov O, Wiedorn MO, et al.: **Synchronous RNA conformational changes trigger ordered phase transitions in crystals**. *Nat Commun* 2021, **12**:1762.
77. Ishigami I, Lewis-Ballester A, Echelmeier A, Brehm G, Zatsepin NA, Grant TD, Coe JD, Lisova S, Nelson G, Zhang S, et al.: **Snapshot of an oxygen intermediate in the catalytic reaction of cytochrome c oxidase**. *Proc Natl Acad Sci U S A* 2019, **116**:3572-3577.
78. Beyerlein KR, Dierksmeyer D, Mariani V, Kuhn M, Sarrou I, Ottaviano A, Awel S, Knoska J, Fuglerud S, Jonsson O, et al.: **Mix-and-diffuse serial synchrotron crystallography**. *IUCrJ* 2017, **4**:769-777.
79. Mehrabi P, Schulz EC, Agthe M, Horrell S, Bourenkov G, von Stetten D, Leimkohl JP, Schikora H, Schneider TR, Pearson AR, et al.: **Liquid application method for time-resolved analyses by serial synchrotron crystallography**. *Nat Methods* 2019, **16**:979-982.
80. Moffat K, Szebenyi D, Bilderback D: **X-ray Laue Diffraction from Protein Crystals**. *Science* 1984, **223**:1423-1425.
81. Tolstikova A, Levantino M, Yefanov O, Hennicke V, Fischer P, Meyer J, Mozzanica A, Redford S, Crosas E, Opara NL, et al.: **1 kHz fixed-target serial crystallography using a multilayer monochromator and an integrating pixel detector**. *Iucrj* 2019, **6**:927-937.
82. Nass K, Bacellar C, Cirelli C, Dworkowski F, Gevorkov Y, James D, Johnson PJM, Kekilli D, Knopp G, Martiel I, et al.: **Pink-beam serial femtosecond crystallography for accurate structure-factor determination at an X-ray free-electron laser**. *IUCrJ* 2021, **8**:15.
83. Eriksson M: **The Multi-Bend Achromat Stroage Rings**. *Proceedings of the 12th International Conference on Synchrotron Radiation Instrumentation (Sri2015)* 2016, **1741**.
84. Wanzenberg R, Agapov I, Brefeld W, Brinkmann R, Chae YC, Chao HC, Keil J, Gavalda XN, Rohlsberger R, Schroer CG, et al.: **Design Status of the Ultra-Low Emittance Synchrotron Facility PETRA IV**. *13th International Conference on Synchrotron Radiation Instrumentation (Sri2018)* 2019, **2054**.
85. Mehrabi P, Bucker R, Bourenkov G, Ginn HM, von Stetten D, Muller-Werkmeister HM, Kuo A, Morizumi T, Eger BT, Ou WL, et al.: **Serial femtosecond and serial synchrotron crystallography can yield data of equivalent quality: A systematic comparison**. *Science Advances* 2021, **7**.
86. Ourmazd A, Moffat K, Lattman EE: **Structural biology is solved — now what?** *Nature Methods* 2022, **19**:3.
87. Inoue K, Koua FH, Kato Y, Abe-Yoshizumi R, Kandori H: **Spectroscopic study of a light-driven chloride ion pump from marine bacteria**. *J Phys Chem B* 2014, **118**:11190-11199.
88. Liebschner D, Afonine PV, Moriarty NW, Poon BK, Sobolev OV, Terwilliger TC, Adams PD: **Polder maps: improving OMIT maps by excluding bulk solvent**. *Acta Crystallogr D Struct Biol* 2017, **73**:148-157.

Annotations

Pandey, S. *et al.* Time-resolved serial femtosecond crystallography at the European XFEL. *Nature methods* **17**, 73-78, doi:10.1038/s41592-019-0628-z (2020).
* The authors report the first TR-SFX experiment at the European XFEL. It is shown how to adjust the XFEL pulse repetition rate to the liquid jet speed, and how it takes for the laser excited jet volume to leave the X-ray interaction region.

Hosseinizadeh, A. *et al.* Single-femtosecond atomic-resolution observation of a protein traversing a conical intersection. *Nature*, doi:doi.org/10.1101/2020.11.13.382218 (2021).
** The precision of TR-SFX has been algorithmically enhanced by machine learning approaches from about 140 fs to a few fs. This way, the transition through the concial intersecition in PYP could be pinpointed to 615 fs, and characterized by tying the parameters of a quantum mechanical calculation to the experiment.

Martin-Garcia, J. M. Protein Dynamics and Time Resolved Protein Crystallography at Synchrotron Radiation Sources: Past, Present and Future *Crystals* **11**, doi:doi.org/10.3390/cryst11050521 (2021).
* This paper provides a comprehensive snapshot of synchrotron based serial crystallographic experiments.

Mehrabi, P. *et al.* Time-resolved crystallography reveals allosteric communication aligned with molecular breathing. *Science* **365**, 1167-1170, doi:10.1126/science.aaw9904 (2019).
* The paper demonstrates how reactions in enzymes can be effectively triggered by using caged substrates. The progress of the reaction is followed by synchrotron based serial crystallography.

Skopintsev, P. *et al.* Femtosecond-to-millisecond structural changes in a light-driven sodium pump. *Nature* **583**, 314-+ (2020).
** TR-SFX with fs time-resolution was applied to a solar driven Na^+ pump. The entire pumping mechanism was recorded from the fundamental isomerization reaction to the end.

Yun, J. H. *et al.* Early-stage dynamics of chloride ion-pumping rhodopsin revealed by a femtosecond X-ray laser. *Proceedings of the National Academy of Sciences of the United States of America* **118**, doi:10.1073/pnas.2020486118 (2021).
** TR-SFX with fs time-resolution was applied to a solar driven, molecular chloride pump. The mechanics of the piston of the pump is revealed in atomic detail.

Carrillo, M. *et al.* High-resolution crystal structures of transient intermediates in the phytochrome photocycle. *Structure*, doi:10.1016/j.str.2021.03.004 (2021).
** The complete Z to E isomerization of a bilin chromophore in a classical bacteriophytochrome (in fact in any biliprotein) is observed by time-resolved crystallography.

Sorigue D et al.: Mechanism and dynamics of fatty acid photodecarboxylase. *Science* 2021, 372.
* This paper shows how a wealth of experimental data obtained by mutiple spectrocopic methods and quantum chemical calculations in combination with TR-SFX can be used to elucidate the function of an enzyme involved in fatty acid synthesis.

Pandey, S. et al.: Observation of substrate diffusion and ligand binding in enzyme crystals using high-repetition-rate mix-and-inject serial crystallography. *IUCrJ* 2021, 8:878-895.
** A Mix-and-inject experiment with single ms time-resolution is reported. The experiment was performed with high X-ray pulse repetition rates at the European XFEL. The formation of the enzyme-substrate complex was observed. Substrate occupancies can be determined in the catalytic cleft of the enzyme at all times and at any location in the microcrystals.

Mehrabi, P. *et al.* Liquid application method for time-resolved analyses by serial synchrotron crystallography. *Nature methods* **16**, 979-982, doi:10.1038/s41592-019-0553-1 (2019).
* Acoustic droplet mix-and-inject serial crystallography at the synchrotron is demonstrated using a fixed target chip on time scales from 30 ms and longer.

Tolstikova, A. *et al.* 1 kHz fixed-target serial crystallography using a multilayer monochromator and an integrating pixel detector. *Iucrj* **6**, 927-937 (2019).
* A multilayer monochromator is used to extract a narrow symmetric energy spectrum from borader undulator X-ray radiation at the European Synchrotron Radiation Facility. Protein crystal diffraction patterns produced by the symmetric X-ray spectrum can be indexed by CrystFEL. Exposure times are less than 5 μs.

Nass, K. *et al.* Pink-beam serial femtosecond crystallography for accurate structure-factor determination at an X-ray free-electron laser. *IUCrJ* **8**, 15, doi:doi.org/10.1107/S2052252521008046 (2021).
* This paper reports the first pink beam (Laue) crystallographic experiment at an XFEL. The number of diffraction pattern necessary for successful SAD phasing and automatic structure building is reduced by a factor of two compared to those required with the nominal SASE bandwidth at XFELs.

Figure Captions

Figure 1. RIs in biological macromolecules. **(a)** Photocycle of the photoactive yellow protein with intermediate states I_T, pR_1, I_{CT}, pR_2, pB_1 and pB_2 whose structures were determined with Laue TRX at the synchrotron. Red dashed box: the *trans* to *cis* isomerization occurs on the ultrafast time scale accessible only to X-ray pulses from an XFEL; pG and pG*: dark (reference) state and electronically exited state, respectively. **(b)** Conformational energy landscape (EL, schematic). The conformational energy (CE, arbitrary units) is presented as a function of two reaction coordinates (rc1 and rc2) which could be for example a bending angle and a rotational angle. Two RIs are depicted. The reaction proceeds through trajectories (dashed arrows, back reactions are ignored) through the EL. Trajectories are usually not accessible by TRX and may be deduced by computational methods. **(c)** Phytochrome photocycle with spectroscopically identified transient states Lumi-R, Meta-Ra, Meta-Rc, Lumi-F and Meta-F. P_r: red light absorbing state; P_{fr}: far-red light absorbing state. Insets show the structural changes of the photosensory core module after light absorption. Slow thermally excited transitions from P_{fr} to P_r are possible (dashed arrow). **(d)** Photocycle of the chloride pumping rhodopsin. The K/L, L/O, O and O/FR' RIs were all characterized spectroscopically[87]. Their absorption maxima are indicated by the subscripts.

Figure 2. *Trans* to *cis* isomerization reactions in Photoactive Yellow Protein (PYP) and in the chloride ion pumping rhodopsin (ClR). **(a) – (c)** *Trans* to *cis* isomerization in PYP. **(a)** The chemical structure of the para-coumaric acid (PCA) in its *trans*-configuration as bound to Cys69 in PYP. The torsional angle φ_T of the $\Delta_{2,3}$ double bond is marked. **(b)** The isomerization reaction of the PCA chromophore as directly observed on the fs time scale. The torsional angle φ_T is plotted (solid spheres) as a function of Δt after reaction initiation by a 140 fs laser pulse (blue arrow). The dashed, black line represents a (step-like) logistics function that follows the φ_T across the transition as a guide to the eye. The isomerization happens around 600 fs during the transition from the electronic excited state potential energy surface (ES-PES, the time-span it is populated is indicated by the red, horizontal bar) to the ground state energy surface (GS-PES, see green, horizontal bar). Inset: chromophore in the *cis*-configuration lined out in red. **(c)** Difference electron density 269 fs and 3 ps after reaction initiation. Negative and positive difference electron densities are shown in red and blue, respectively (3 sigma level). The dark state (reference) model is shown in yellow; the PYP structure at 269 fs is shown in pink and that at 3 ps in green. The $\Delta_{2,3}$ double bond is marked by a red arrow on the left. The *trans* and *cis* configurations are apparent. **(d-e)** The *trans* to *cis* isomerization in the chloride ion pumping rhodopsin (ClR). **(d)** The chemical structure of retinal bound to Lys235 in ClR. Isomerization occurs about the $\Delta_{13,14}$ double bond (red arrow). The torsional angle of the $\Delta_{13,14}$ double bond is marked. The Schiff base is marked in green. **(e)** Overall structure of ClR. The Cl^- ion is pumped across the membrane from the extracellular to the cytoplasmic

side. The seven transmembrane helices (A-G) of the rhodopsin are marked. Helix G is cut open from residues 225 to 234 to allow an unperturbed view on the retinal (marked as ret) and the Schiff base. In the dark, Cl^- (green) interacts with the Schiff base. The retinal (yellow) is in its $\Delta_{13,14}$ *trans* configuration. After light illumination the retinal isomerizes about the $\Delta_{13,14}$ double bond to *cis* (green structure). The *cis*-configuration is shown in transparent red. φ_T is marked. After 1 ps the Cl^- (red sphere) is released, and moves initially towards the extracellular side (red, dashed arrow). The isomerization causes the Schiff-base nitrogen to turn away to prevent the interaction with Cl^-. Difference electron density is localized to the position of the Schiff base and the Cl^- and is shown in red (negative, -3 sigma) and green (positive, 3 sigma).

Figure 3. *Z* to *E* isomerizations in bacterial phytochromes (BphPs). **(a)** Structure of the SaBphP2 photosensory core module (PCM) overlayed onto a difference map (2.7 sigma contour level for negative, green and positive, red difference features) obtained at 5 ns. The chromophore pocket is marked by the red box and shown enlarged within the dotted box. The PAS, GAF and PHY domains are marked and depicted in yellow, green and magenta respectively. The red arrow denotes the beginning of a long helix that connects the PHY domain to the effector domain with enzymatic activity. The smaller chromophore binding domain lacks the PHY domain. **(b)** The chemical structure of the biliverdin chromophore bound to the BphP. The D-ring is in the *Z* (*cis*) configuration; the torsional angle φ_T is marked in red. **(c)** Observed difference electron density near the BV 5 ns after light absorption. Red/green: negative/positive difference electron density, respectively, on the 3 sigma level. The pyrrole water (PW) is photo-ejected. The D-ring occupies two conformations (light blue and orange), one with a φ_T of 72°, and another with φ_T of 172° (see inset), the D-ring rotates clockwise if viewed along the axis of BV rings D to B. The structure of the dark/ reference state is shown in gray. Inset: extrapolated electron density (blue) supports the two structural intermediates shown in blue and orange. The D-ring (orange structure) is in the *E* (*trans*) configuration.

Figure 4. Reaction of BlaC with Ceftriaxone (CEF). **(a)** Overall BlaC structure with 4 subunits in the asymmetric unit. Transparent boxes: catalytic centers. **(b)** Fractional concentrations of the enzyme substrate complex (BlaC-CEF) in the platelet microcrystals at 5 ms. Blue: low occupancies < 5 %, pink and gray hues: high occupancies. Red dashed line and below: central cross-section. **(c)** Fractional concentrations of BlaC-CEF at 10 ms; colors as in (b). Red dashed line and below: central cross-section. **(d) – (i)** Reaction of CEF with BlaC shown in the catalytic cleft of BlaC subunit B (red box in (a)). Some important amino acids and the P_i are marked in (d); **(e-g)** data are collected at the European XFEL; difference electron density is shown as Polder maps[88] (blue, 3 sigma contour level); **(h-i)** data are collected at the LCLS; mFo-DFc omit-difference maps are shown in green (2.7 sigma contour level). **(d-f)** BlaC-CEF complex formation, **(g-h)** fully evolved enzyme substrate complex, **(i)** catalytic reaction, formation of the acyl-complex by establishing a covalent bond (red arrow) between the catalytic Ser-70 and the CEF. The leaving group present in intact CEF (grey) is cleaved off (black arrow).

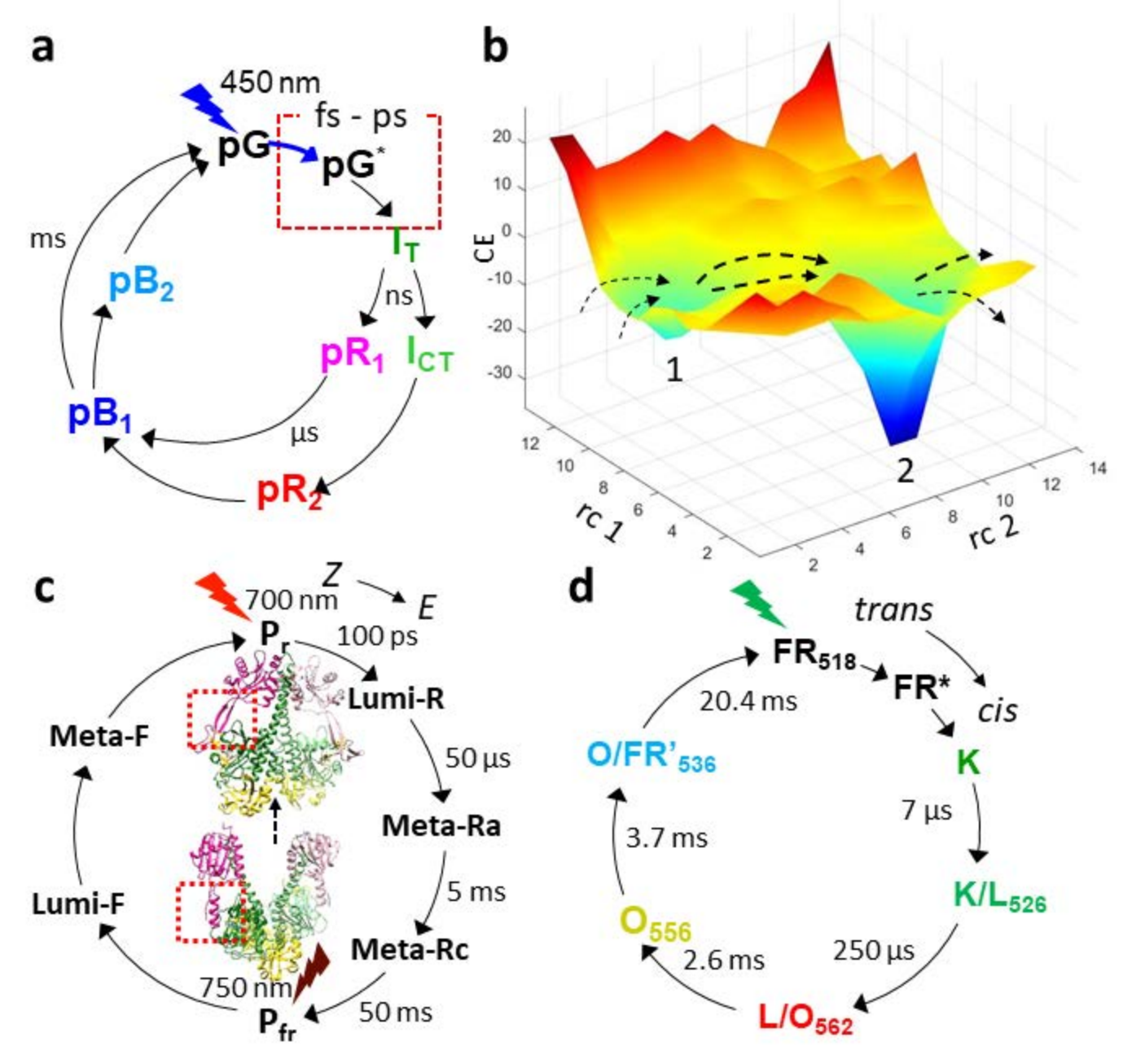
a
450 nm
fs - ps
pG
pG*
I_T
ns
pR_1
I_{CT}
pB_2
ms
pB_1
µs
pR_2
b
CE
20
10
0
-10
-20
-30
1
2
rc 1
rc 2
12
10
8
6
4
2
14
c
700 nm
Z
E
P_r
100 ps
Lumi-R
50 µs
Meta-Ra
5 ms
Meta-Rc
50 ms
P_{fr}
750 nm
Lumi-F
Meta-F
d
trans
FR_{518}
FR*
cis
20.4 ms
O/FR'_{536}
K
7 µs
3.7 ms
K/L_{526}
O_{556}
2.6 ms
250 µs
L/O_{562}

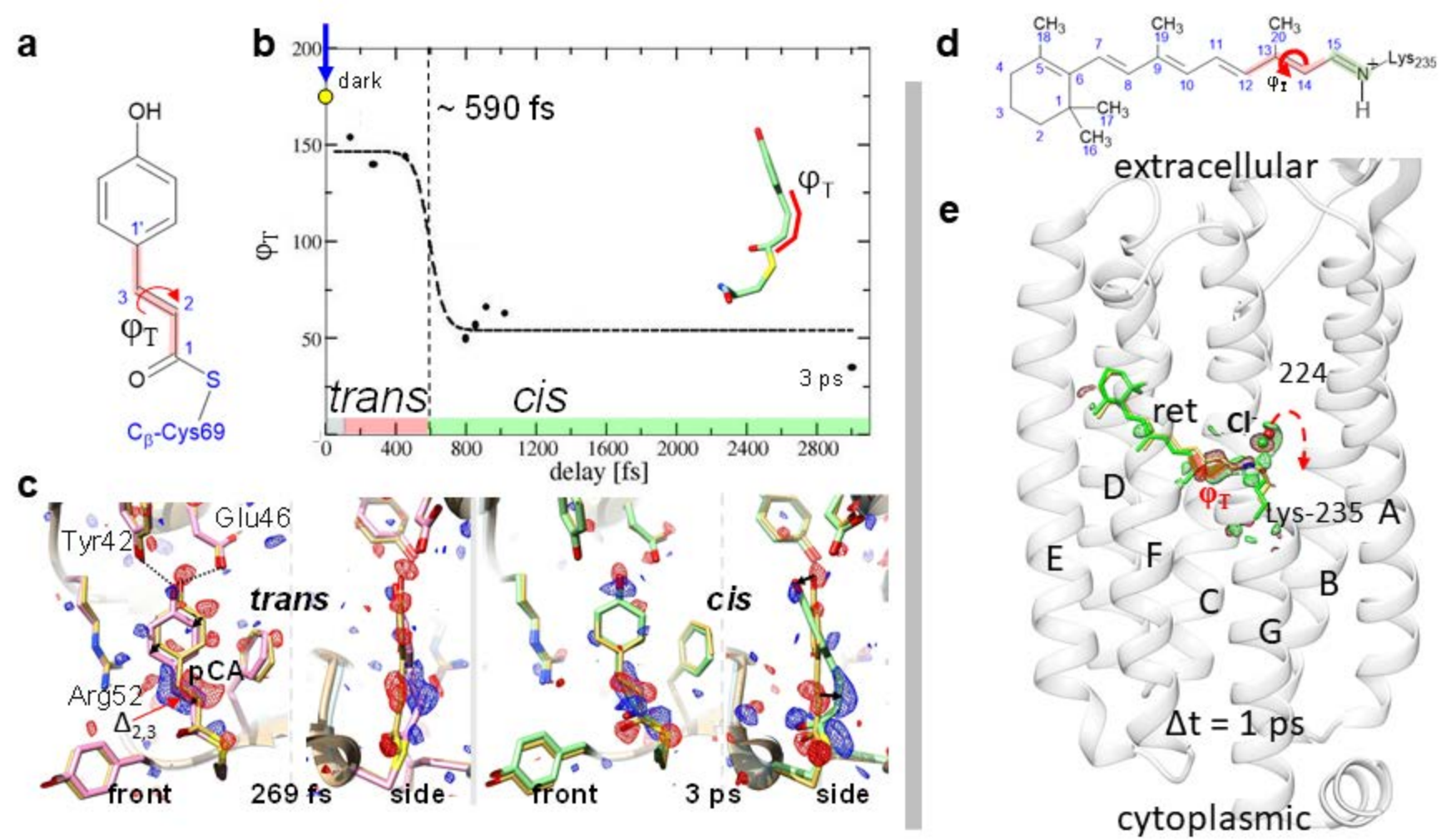
a
OH
1'
3
2
φT
1
O
S
Cβ-Cys69
b
200
dark
~ 590 fs
150
φT
100
50
trans
cis
3 ps
0
400
800
1200
1600
2000
2400
2800
delay [fs]
φT
c
Tyr42
Glu46
trans
pCA
Arg52
Δ2,3
front
269 fs
side
cis
front
3 ps
side
d
CH3
18
7
19
11
20
131
15
Lys235
4
5
6
8
9
10
12
φT
14
N
H
1
3
CH3
17
2
CH3
16
e
extracellular
224
ret
cl
D
φT
Lys-235
A
E
F
B
C
G
Δt = 1 ps
cytoplasmic

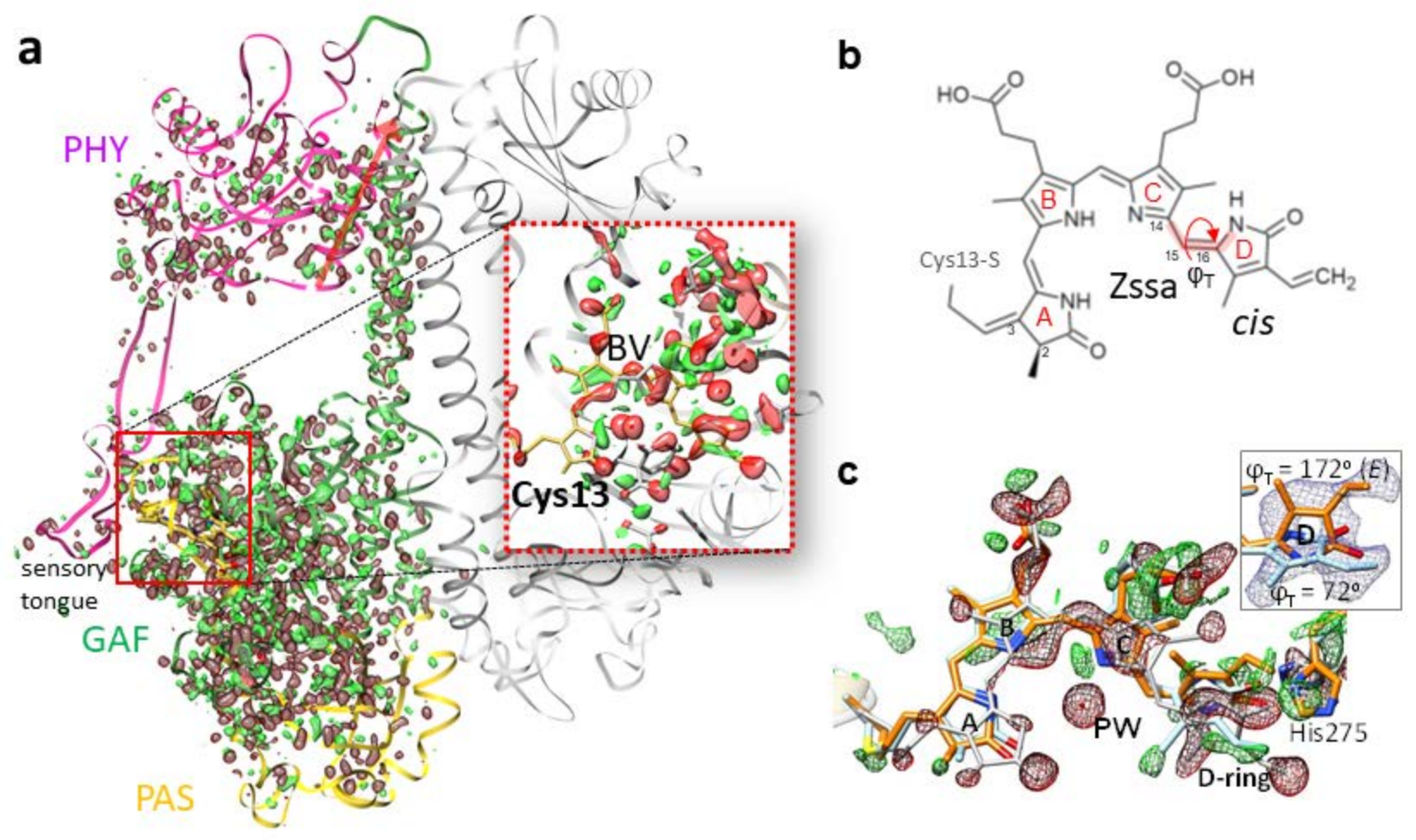
a
PHY
BV
Cys13
sensory
tongue
GAF
PAS
b
HO
OH
B
C
D
A
NH
Cys13-S
Zssa
φ_T
cis
CH_2
c
φ_T = 172° (E)
φ_T = 72°
PW
His275
D-ring

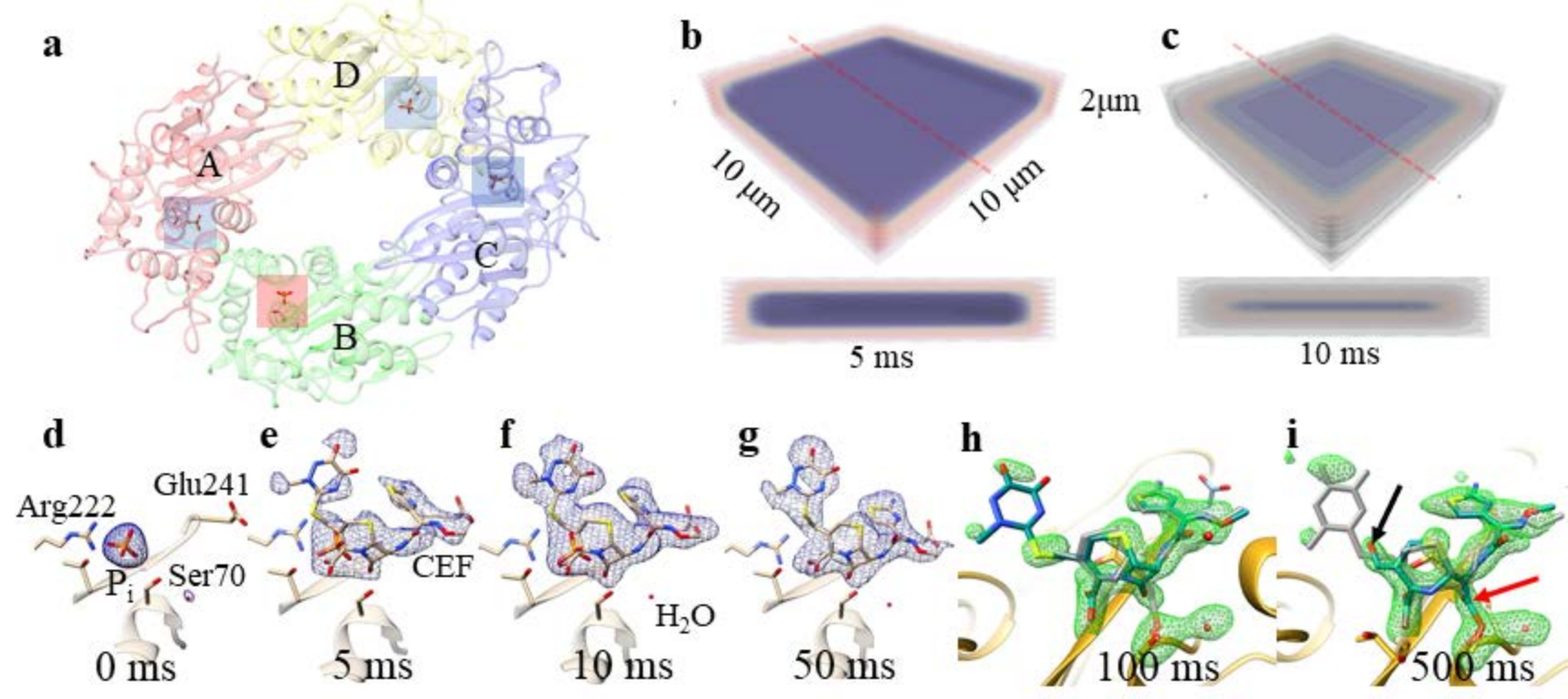
a
D
A
C
B
b
2μm
10 μm
10 μm
5 ms
c
10 ms
d
Arg222
Glu241
P_i
Ser70
0 ms
e
CEF
5 ms
f
H_2O
10 ms
g
50 ms
h
100 ms
i
500 ms